URSI GASS 2023, Sapporo, Japan, 19 – 26 August 2023

Scattered Field Polarization for VLF Remote Sensing of Transient Events

Hunter C. Burch*(1)(2) and Robert C. Moore(2)
(1) Auburn University, Auburn, AL, USA; e-mail: hcburch@auburn.edu
(2) University of Florida, Gainesville, FL, USA; e-mail: moore@ece.ufl.edu

Abstract

Very low frequency (VLF, 3−30 kHz) radio waves can propagate large distances around the globe in the Earth-ionosphere waveguide and be scattered by transient disturbances to the lower ionosphere. Such scattering enables the VLF remote sensing of lightning-related (as well as other) disturbances to the *D*-region ionosphere (60−100 km altitude). The polarization of the field scattered by the ionospheric disturbance has not been investigated in detail, primarily because it can be difficult to measure. In this paper, we present a simple, reliable method to accurately calculate the polarization of such a scattered field, and we apply the method to analyze ionospheric VLF scattering events.

1 Introduction

Measurements of the amplitude, phase, and polarization of a propagating very low frequency (VLF) radio wave have been applied to a wide variety of geospace-related events [1]–[3]. When a sudden, localized disturbance occurs in the ionosphere between a VLF transmitter and receiver, the received signal is affected for a period of time, after which it recovers to (nearly) its original value. Such transients can be produced by a wide variety of events, including lightning (e.g., early/fast events, long recovery events, and lightning induced electron precipitation events), solar flares and eclipses [2], or even galactic γ-ray bursts.

Early/fast events occur within 20 ms of an associated lightning flash, and the VLF signal perturbations reach a peak within 20 ms of the event onset. Long recovery early events (LOREs) exhibit the same onset characteristics as early/fast VLF events, but can take tens of minutes to recover [4]. Slow variation of the ambient ionosphere presents a major difficulty in measuring the properties of long recovery events [5]. The scattered field polarization measurement described in this paper produces accurate results even when the ambient field varies during the event.

Lightning-induced electron precipitation (LEP) occurs when an electromagnetic pulse from terrestrial lightning propagates into the magnetosphere [6] and resonantly scatters energetic electrons trapped in Earth's radiation belts, causing some electrons to precipitate into the Earth's upper atmosphere [6], [7]. LEP events are under current investigation [8], [9], with particular interest in ducted vs. non-ducted events. Ducted LEP events are expected to remain relatively stationary, whereas non-ducted LEP events are expected to progress poleward over the course of the event [10].

Scattered field analysis of the form championed by *Dowden et al.* [11] and revitalized by *Kotovsky and Moore* [12] conceives of received signal as the addition of a scattered field from the disturbance to the existing ambient field at the receiver. Past analysis of the scattered field has focused on the change in amplitude and phase on a single channel. This paper demonstrates a method to measure the scattered field simultaneously on two channels using the Stokes polarization parameters [13] and presents for the first time scattered field polarization analysis of a variety of transient disturbances along with the insight gained over standard scattered field-only or polarization-only analysis.

2 Scattered Field Polarization

Consider a subionospherically-propagating VLF transmitter signal received simultaneously on two orthogonal horizontal magnetic field antennas and composed of an ambient field with amplitude A and phase ϕ, and a scattered field from an ionospheric disturbance with magnitude B and angle ψ. The total horizontal magnetic field at the receiver may be expressed as:

$$\begin{aligned}\mathbf{H_x}+\mathbf{H_y} = &\left(A_x\exp(j\phi_x)+B_x\exp(j\psi_x)\right)\mathbf{x}+\\ &\left(A_y\exp(j\phi_y)+B_y\exp(j\psi_y)\right)\mathbf{y}\end{aligned} \quad (1)$$

For a signal with an ambient and scattered field added at the receiver, Equation 2 gives an expression for the waveguide Stokes parameters of the total field in terms of the amplitude and phase of the ambient field, and magnitude and angle of the scattered field, calculated in the manner of *Burch and Moore* [3]. In practice, the magnitude B of the scattered field may be considered zero before the onset and after the recovery of a VLF event. Thus, the change in each parameter from baseline after the onset of the event, ΔS_{0-3} may be interpreted as the difference in the Stokes parameters of the total and ambient fields, $(S_{0-3})_t - (S_{0-3})_a$. Applying this terminology and the definitions of the ambient and scattered field Stokes parameters yields the expressions in Equation 3.

$$
\begin{aligned}
S_0 =& A_x^2 + A_y^2 + B_x^2 + B_y^2 + \\
& 2A_xB_x\cos(\psi_x - \phi_x) + 2A_yB_y\cos(\psi_y - \phi_y) \\
S_1 =& A_x^2 - A_y^2 + B_x^2 - B_y^2 + \\
& 2A_xB_x\cos(\psi_x - \phi_x) - 2A_yB_y\cos(\psi_y - \phi_y) \\
S_2 =& 2A_xA_y\cos(\phi_x - \phi_y) + 2A_xB_y\cos(-\psi_y + \phi_x) + \\
& 2A_yB_x\cos(\psi_x - \phi_y) + 2B_xB_y\cos(\psi_x - \psi_y) \\
S_3 =& 2A_xA_y\sin(\phi_x - \phi_y) + 2A_xB_y\sin(-\psi_y + \phi_x) + \\
& 2A_yB_x\sin(\psi_x - \phi_y) + 2B_xB_y\sin(\psi_x - \psi_y)
\end{aligned} \tag{2}
$$

$$
\begin{aligned}
\Delta S_0 =& (S_0)_s + 2A_xB_x\cos(\psi_x - \phi_x) + \\
& 2A_yB_y\cos(\psi_y - \phi_y) \\
\Delta S_1 =& (S_1)_s + 2A_xB_x\cos(\psi_x - \phi_x) - \\
& 2A_yB_y\cos(\psi_y - \phi_y) \\
\Delta S_2 =& (S_2)_s + 2A_xB_y\cos(-\psi_y + \phi_x) + \\
& 2A_yB_x\cos(\psi_x - \phi_y) \\
\Delta S_3 =& (S_3)_s + 2A_xB_y\sin(-\psi_y + \phi_x) + \\
& 2A_yB_x\sin(\psi_x - \phi_y)
\end{aligned} \tag{3}
$$

Using measurements of the total field Stokes parameters and estimates of the ambient field Stokes parameters, we apply the Levenberg-Marquardt algorithm as implemented by MATLAB's *fsolve* function to solve the system of nonlinear equations in Equation 3 and choose the values of B_x, B_y, ψ_x and ψ_y that best match the observed change in each Stokes parameter. Without loss of generality (for calculation of the scattered field Stokes parameters), the phase of the ambient field on one channel is taken to be zero and the phase on the other channel is $\Delta\phi = \angle(\mathbf{H_x H_y}^*)$ before the onset of the event. A_x, A_y, and $(S_{0-3})_a$ are estimated using measurements of the field before the onset and after the recovery of each event.

In the following sections, we demonstrate the utility of this technique by applying it selected VLF events that would be difficult to analyze using conventional scattered field techniques.

3 Long Recovery Early VLF Event

VLF amplitude and phase perturbations associated with a long recovery event (LORE) are shown in Figure 1. The transmitter signal phase is changing before the event onset and does not recover to the starting value. The signal amplitude also appears to be in flux, as the North/South channel amplitude returns to the starting value around 03:30 UTC but the East/West channel amplitude does not return to its start value until nearly 03:40 UTC. Conventional scattered field analysis would require the estimation of a changing ambient field value throughout the course of the event, and the selection of ambient amplitude and phase estimates would impact the apparent recovery characteristics on each channel.

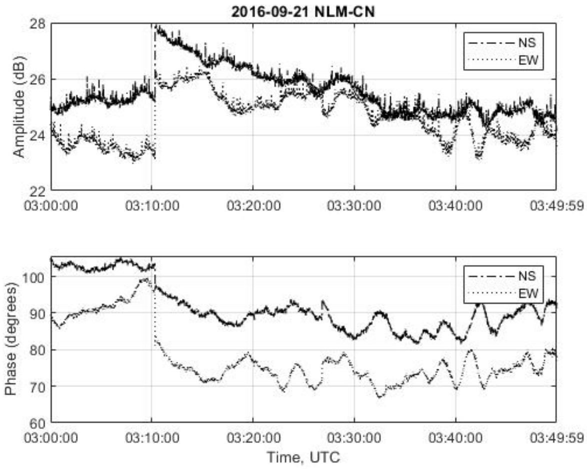

Figure 1. Amplitude and phase measurements of a long recovery event on the LaMoure, North Dakota VLF transmitter signal recorded near Chapel Hill, North Carolina.

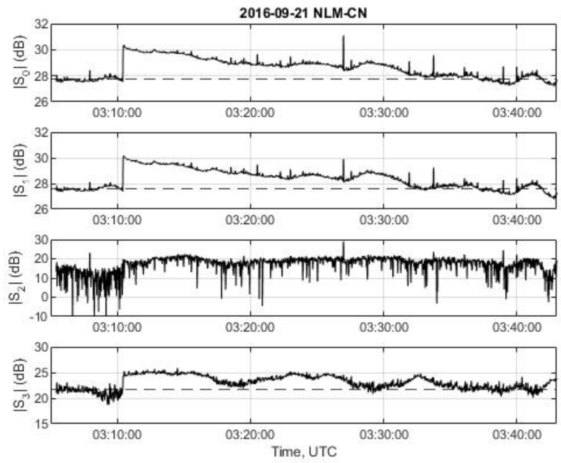

Figure 2. Waveguide Stokes parameters of the LaMoure, North Dakota VLF transmitter signal recorded near Chapel Hill, North Carolina during a long recovery event.

The Stokes parameters of the total field, shown in Figure 2, all exhibit the same onset time and recover to the start value (dashed line) at around the same time (approximately 03:40 UTC, giving the total time of the LORE from onset to recovery at about 30 minutes). The Stokes parameters in Figure 2 are given with respect to the direction of highest signal to noise ratio (SNR) for the transmitter.

Figure 3 shows the normalized scattered field magnitude rotated into the direction of highest SNR and normalized by the high-SNR ambient field, with a distinctly different pattern of onset and recovery on the high- and low-SNR channels. While the scattered field on the high-SNR channel demonstrates a sharp onset and relatively smooth recovery, the low-SNR channel shows a low, constant value of the scattered field after onset until the end of the event.

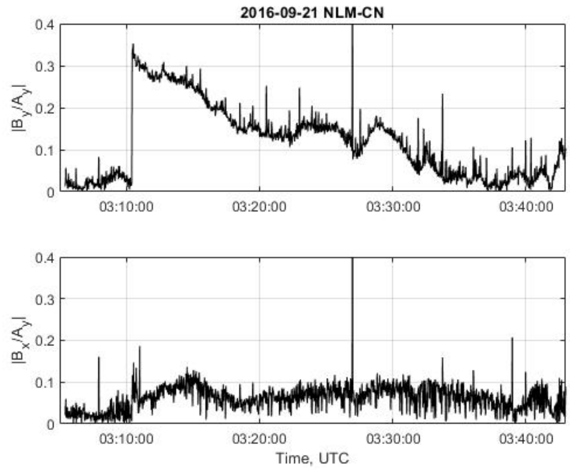

Figure 3. Normalized scattered field magnitude of the LaMoure, North Dakota VLF transmitter signal recorded near Chapel Hill, North Carolina during a long recovery event.

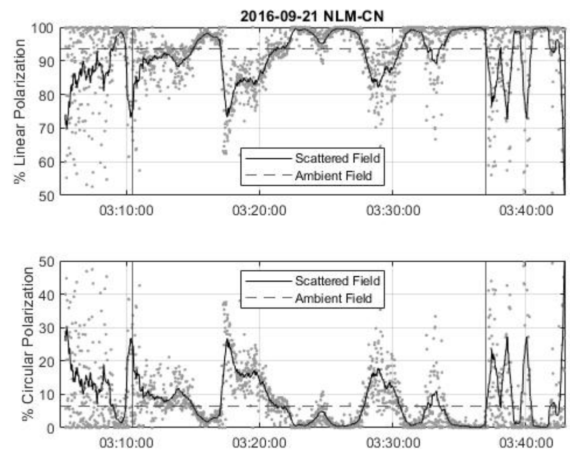

Figure 4. The proportion of linear- and circular-polarized signal content in the scattered field of the LaMoure, North Dakota VLF transmitter signal recorded near Chapel Hill, North Carolina during a long recovery event.

The Stokes parameters of the scattered field may be analyzed to determine the relative proportion of linear- and circular-polarized signal content. The percentage of circular-polarized content is $(S_3/S_0)^2 * 100\%$. The remaining signal content is linear-polarized, with a percentage given by $(S_1^2 + S_2^2)/S_0^2 * 100\%$. Figure 4 compares the percentage of linear- and circular-polarized signal content at a 1 Hz sample rate, with 30-second averages shown by the black line. The polarization of the estimated ambient field is shown with a dashed line. While the scattered field is dominantly linear-polarized (80-100% throughout the event), the proportion of circular-polarized signal content surges three times to 20-30%. It appears that additional events are occurring during these pulses. We can be sure that the timescale for recovery is valid, however, as can be calculated from the first 7 minutes of the event with no interference.

It is particularly interesting to note that while Figure 4 shows three repeated pulses of increased circular polarization, Figure 3 only shows two associated increases in the scattered field magnitude (one at the event onset at around 03:10 UTC, and another at around 03:27 UTC, which is also visible in the phase of Figure 1). The change in scattered field polarization visible at 03:17 UTC in Figure 4 may be attributed to an additional scattered field from an event that would have otherwise been drowned out by the ongoing long recovery event.

4 Lightning-Induced Electron Precipitation Event

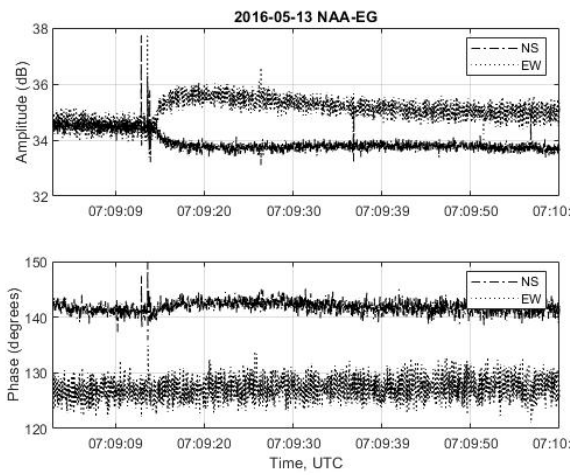

Figure 5. Amplitude and phase measurements of an LEP event on the Cutler, Maine VLF transmitter signal recorded near East Granby, Connecticut.

Figure 5 shows a perturbation of the Culter, Maine VLF transmitter (callsign NAA) recorded near East Granby, Connecticut which exhibits features characteristic of a lightning-induced electron precipitation (LEP) event, with a strong lightning sferic detected 1-2 s before the onset of the perturbation.

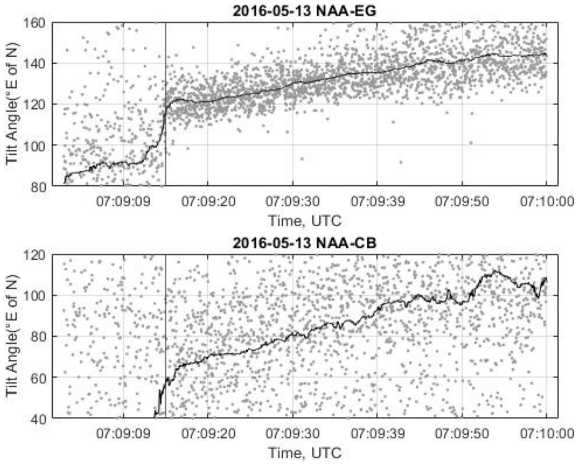

Figure 6. The tilt angle of the scattered field of the Cutler, Maine VLF transmitter signal recorded near East Granby, Connecticut (top) and Camp Blanding, Florida (bottom) during an LEP event.

The scattered field estimation method was applied to the measured Stokes parameters for the event at both the East Granby, Connecticut, and Camp Blanding, Florida, receivers. Unusually, the stronger scattered field appears on the low SNR channel for this event. This would suggest that the source of the scattered field was at a location far off-path, unlike the long recovery event also presented in this paper.

The scattered field recorded at East Granby was $75-85\%$ linear-polarized, and the scattered field recorded at Camp Blanding was $85-95\%$ linear-polarized over the course of the event. Figure 6 shows the tilt angle of the linear-polarized portion of the signal at each of the two sites over time at 50 Hz sampling, with the black line showing a tilt angle calculated using a 5 s moving average of the scattered field Stokes parameters. The tilt angle is calculated as the angle of $(S_1 + jS_2)/2$, and may be interpreted as an apparent direction of arrival for the linearly-polarized signal.

Kim [9] suggested that the interhemispheric timing of ducted and non-ducted LEP events would be significantly different, but experimentally detecting the difference would require an array of VLF receivers in both northern and southern hemispheres. The tilt angles shown in Figure 6 clearly indicate that the effective center of the ionospheric disturbance in this case is moving with time. It thus appears that the polarization of the scattered field provides a single-site means to distinguish between non-ducted and ducted LEP events, allowing for interhemispheric LEP timing statistics to be evaluated using single-site observations.

Acknowledgments

Support was provided by DARPA grants HR00111820013 and HR001121C0081 to the University of Florida.

References

[1] H. Voss, W. Imhof, M. Walt, *et al.*, "Lightning-induced electron precipitation," *Nature*, vol. 312, no. 5996, pp. 740–742, 1984.

[2] R. Moore and H. Burch, "The d region response to the august 2017 total solar eclipse and coincident solar flare," *Geophysical Research Letters*, vol. 45, no. 24, pp. 13–192, 2018.

[3] H. Burch and R. C. Moore, "The relationship between "large" early/fast vlf events and modal propagation nulls," *IEEE Transactions on Geoscience and Remote Sensing*, vol. 60, pp. 1–7, 2022.

[4] D. Kotovsky and R. Moore, "Modeling long recovery early events (lores) produced by lightning-induced ionization of the nighttime upper mesosphere," *Journal of Geophysical Research: Space Physics*, vol. 122, no. 7, pp. 7761–7780, 2017.

[5] C. Haldoupis, M. Cohen, E. Arnone, B. Cotts, and S. Dietrich, "The vlf fingerprint of elves: Step-like and long-recovery early vlf perturbations caused by powerful±cg lightning em pulses," *Journal of Geophysical Research: Space Physics*, vol. 118, no. 8, pp. 5392–5402, 2013.

[6] R. A. Helliwell, *Whistlers and related ionospheric phenomena*. Stanford University Press Stanford, Calif., 1965, vol. 50.

[7] J. Bortnik, "Precipitation of radiation belt electrons by lightning-generated magnetospherically reflecting whislter waves," Ph.D. dissertation, Stanford University, 2005.

[8] M. Gołkowski, N. Gross, R. Moore, B. Cotts, and M. Mitchell, "Observation of local and conjugate ionospheric perturbations from individual oceanic lightning flashes," *Geophysical Research Letters*, vol. 41, no. 2, pp. 273–279, 2014.

[9] D. Kim, "Analysis of conjugate lightning-induced electron precipitation events using the vlf remote sensing method," Ph.D. dissertation, University of Florida, 2020.

[10] D. S. Lauben, U. S. Inan, and T. F. Bell, "Poleward-displaced electron precipitation from lightning-generated oblique whistlers," *Geophysical Research Letters*, vol. 26, no. 16, pp. 2633–2636, 1999.

[11] R. L. Dowden, J. B. Brundell, and C. J. Rodger, "Temporal evolution of very strong trimpis observed at darwin, australia," *Geophysical Research Letters*, vol. 24, no. 19, pp. 2419–2422, 1997.

[12] D. Kotovsky and R. Moore, "Classifying onset durations of early vlf events: Scattered field analysis and new insights," *Journal of Geophysical Research: Space Physics*, vol. 120, no. 8, pp. 6661–6668, 2015.

[13] G. G. Stokes, "Xxx. on the change of refrangibility of light," *Philosophical transactions of the Royal Society of London*, no. 142, pp. 463–562, 1852.